

Optimization of excitation of fibre Fabry-Perot tunable filters used in swept lasers using a phase correction method

MOHAMMAD. R. N. AVANAKI^{1,2,3,*}, ADRIAN BRADU⁴ AND ADRIAN PODOLEANU⁴

¹Department of Biomedical Engineering, Wayne State University, Detroit, Michigan, USA

²Department of Dermatology, Wayne State University School of Medicine, Detroit, Michigan, USA

³Barbara Ann Karmanos Cancer Institute, Detroit, Michigan, USA

⁴Applied Optics Group (AOG), School of Physical Sciences, University of Kent, Canterbury, Kent, CT2 7NH, United Kingdom

*Corresponding author: mrn.avanaki@wayne.edu

In this paper, we investigate a phase correction method for compensation of the nonlinearity of conventional wavelength swept laser sources based on a fiber Fabry-Perot tunable filter as a wavelength selective element. A triangular waveform signal is commonly used to drive the filter. We however extract the zero crossings from the interferograms and modify the shape of the triangular signal accordingly. This algorithm was tested for different values of the optical path length difference (OPD) in the interferometer set-up. Significant compensation for the non-linearity of the filter was obtained.

1. INTRODUCTION

Most wavelength swept laser sources (SS) that use a scanning Fabry-Perot tunable filter (FP-TF) exhibit a nonlinear temporal change of frequency due to the typically sinusoidal excitation applied to the piezoelectric (PZT) controlled filter [1-3]. Even if the excitation signal is triangular, the response of the filter can still be non-linear. Ideally, a linear arrangement of data along the k-axis (in wavenumber) is required prior to Fast Fourier Transformation (FFT) in order to yield a correct depth profile [4, 5]. Incorrect optical frequency mapping leads to an A-scan with broadened peaks, that exhibits distortions similar to those due to dispersion left uncompensated [6, 7]. Usually, for a linear excitation of the tunable filter in the form of a triangular signal at slow speeds, the frequency generated varies linearly in time [8-10]. This regime does not require any k-trigger or wavelength re-sampling process. However, the higher the frequency of the excitation waveform, the larger the deviation of the mechanical response of the FP from the applied waveform. Therefore, a re-sampling mechanism prior to FFT is required [1, 11].

To compensate for the filter nonlinearities, various solutions were proposed. (1) Using a software approach, by re-sampling the data after analogue-to-digital conversion (A/D) [12]. Several signal processing methods have recently been studied addressing the issue of maintaining excellent image performances by reducing the non-linearity of the filter while minimizing the computational time [12]. (2) Using a hardware approach, by clocking the A/D with an electronic trigger-signal (K-trigger) generated by an interferometer [13, 14]. This solution works well, however it increases the overall cost of the system. (3) Another

solution to correct for nonlinearity of such optical sources was implemented recently for a swept source Fourier domain mode locked laser [15-18]. The procedure for the correction is as follows. The complex response function of the FP-TF is characterized and a superposition of sinusoidal waveforms at the first three harmonics of the filter resonance frequencies is generated. The ideal parameters combination for these waveforms is found using a numerical iterative optimization algorithm with 7 variables (amplitudes and phases of the three harmonics and the centre wavelength offset). We have also devised a solution close to this, based on generating a synthesized anti-phase modulation waveform in order to reduce the nonlinearities of the filter [11, 19]. In this approach, the waveform is found experimentally during an iterative hardware adjustment/optimization process. The parameters that need to be optimized are frequency, amplitude and phase of a burst signal applied in addition to the triangular signal. The resulting waveform applied to the FP-TF is a quasi-arbitrarily synthesized waveform. The adjustment is performed more based on the amplitude and phase of the bursts and less on the number of cycles in the bursts [11].

2. MATERIALS AND METHODS

2.1. Experimental SS-OCT set-up

An FP-TF swept source laser has been devised and used with an optical coherence tomography (OCT) imaging instrument. The fibered source is coupled to the OCT system, designed as a Mach-Zehnder fibre interferometer constructed with two directional couplers (DC). To avoid light being sent back into the source, the coupling is performed via

an optical isolator (ISO). Part of the light is sent via a bulk beam splitter (BS) to the sample arm comprising a pair of orthogonal galvo-scanners and interface optics for three dimensional imaging. To compensate for unbalanced dispersion in the interferometer, rods of optical glass are used in the interferometer's reference arm. These are incorporated here into the block "Optical compensator" in Fig. 1. The backscattered signal from the sample is coherently recombined with the signal from the reference arm at the directional coupler. The OPD value is adjusted using a translation stage (TS). The interference signal is detected using a balanced photo-detector (Newfocus, 80 MHz electronic bandwidth), with internal adjustable gain. More details of the design of this system are described in [11] and [22].

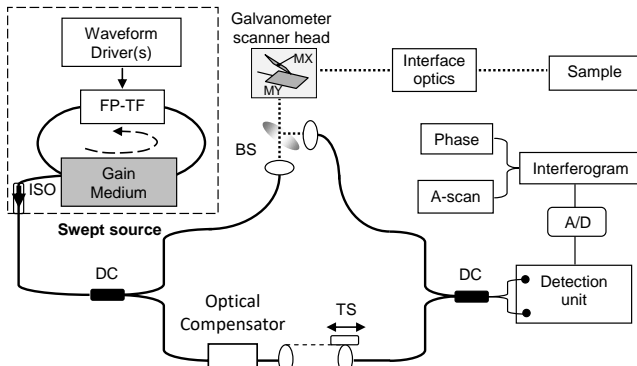


Fig. 1. Experimental SS-OCT set-up. DC: directional couplers, BS: beam splitter, TS: translation stage, A/D: analogue to digital converter, FP-TF: Fabry-Perot tunable filter, ISO: optical isolator.

A swept source with a central wavelength of $\lambda_0 = 1050$ nm was used. We measured the tuning bandwidth of the swept source as 25 nm using an optical spectrum analyzer when the excitation signal applied to the filter is a triangular signal with 10V peak to peak and +6V offset (see Fig. 2).

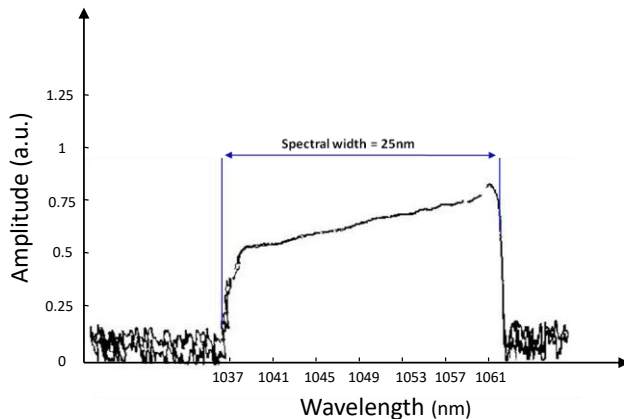


Fig. 2. Spectral width of the swept source, measured by an optical spectrum analyser.

Conventional swept laser sources, as depicted in Fig. 1, are configured as optical resonators that include a fast dynamic gain medium (a solid-state optical amplifier (SOA)). The laser source used in this study was provided by Superlum, SOA-522. The high speed tuning wavelength element placed inside the resonating cavity was a Fabry-Perot tunable filter (FP-TF) produced by Lambda Quest™, LQ-H231. A feature that makes FP-TF devices attractive for this type of laser is their all-fibre

optics platform. Such a combination gives high performance, reliability, low cost, and design flexibility, which allows customization to achieve different spectral regions, sweep range, coherence length, and power level [5, 20-21].

The shape of the signal sent to the tunable filter is a triangular signal. The amplitude and offset of the signal determine the tuning bandwidth and the centre frequency, respectively. The frequency of the waveform determines the tuning rate of the source or the A-scan acquisition speed of the OCT system. Similar circuitry to that reported before [21] was employed. This employed a PCI-6110, 12-bit PCI input/output DAQ card from National Instrument, together with a SH68-68EP cable and BNC-2110 connector block. The input and output rates used in this study are 5MS/s and 1.5MS/s, respectively. The acquisition hardware of the compensation/optimization system is shown in Fig. 3.

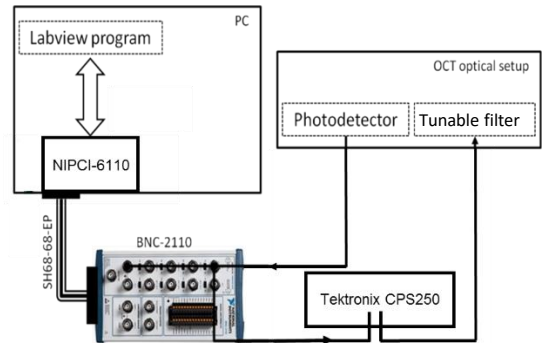


Fig. 3. Hardware of the compensation system. The solid black lines in the diagram represent coaxial BNC cables.

The FP filter needs to be driven by a certain amplitude and offset to employ its full sweeping range. The amplitude of the triangular signal (10 V peak to peak) and the offset voltage (+6V) are obtained experimentally. The DAQ (NI PCI-6110) can generate voltages between -10 V and +10 V. To generate voltages outside this range a DC power supply (Tektronix, CPS250) was used in series with the output port of the PCI-6110 (see Fig. 3). The power supply adds +1V to the triangular signal and raises the peaks to +1V and +11V when the DAQ generates voltages between 0 and 10 V. There is a risk of possible damage to the filter or other devices if the grounding of the instruments is not done carefully. To generate the offset waveform, a Bias-T is used to combine the AC and DC waveform. The resultant triangular signal is ready to be sent to the FP filter through the output port of the BNC-2110 (AO0). An interferogram is acquired by the input port of the BNC-2110 (AIO) through PCI-6110. The interferogram is altered according to the shape of the modified triangular signal. The signal is processed by a phase correction algorithm that is implemented in LabVIEW.

2.2. Phase correction algorithm

The method evaluated here to compensate for the filter nonlinearities differs from the methods mentioned above. The aim is to make the zero crossings of the interferogram signal equidistant. In this method, the zero crossings are extracted from the interferogram and the shape of the ramp signal is modified accordingly, in order to compensate for the distances between the zero crossings. Similar to the idea introduced in our previous method [21], a ramp signal can be composed of several short lines that their slopes can vary. Each short line is constructed from several data samples. Decreasing the slope of the short lines of the ramp signal, increases the distance between the zero crossings of the interferogram signal, whereby increasing the slopes the distance between the zero crossings is decreased. The algorithm of the phase correction method is as follows. Initially, the

number of samples obtained by digitizing the photo-detected signal is increased by a factor of 10 using a cubic Spline interpolation method. A spline is a sufficiently smooth piecewise-polynomial function. We used "Spline Interpolation 1D" virtual instrument (VI) in LabVIEW which is an one dimensional spline. The VI performs based on a lookup table defined by X and Y . This VI accepts tabulated X and Y values (independent and dependent variables, respectively) and provides interpolated values y_i that correspond to each x_i location. The VI looks up each value of x_i in X and uses the relative location in X to find the interpolated value y_i at the same relative location within Y . The zero crossings of the up-sampled interferogram signal are then determined. The zero crossing profile is generated based on the distance between the zeros. Before applying the zero crossing algorithm, the interferogram was adjusted vertically around zero using four consecutive windows along the sample index axis. This was done to find a more accurate distance between the zeros. According to the zero crossing profile the ramp signal is modified to the signal in which, each sample's slope is calculated as unity (the slope of a ramp signal) plus the slope obtained from the zero crossing profile for that sample. We have also modified the ramp signal using another approach in which, each sample value is constructed by the slope obtained from the zero crossing profile. The formulae for modifying the ramp signal using these two methods are given below (equations (1), (2)). $slope_add$ in the formulae, is a variable showing the slope obtained from the zero crossing profile.

$$sample(i) = sample(i - 1) + i * slope_add \quad (1)$$

$$sample(i) = i * (1 + slope_add) \quad (2)$$

The obtained ramp signal has the same number of samples as the up-sampled interferogram has. The number of samples is given by the frequency of the ramp signal. For instance for a ramp signal at 7.2 kHz, 100 samples are required. The ramp signal produced in this way is then sent to the FP-TP filter.

3. RESULTS

In this section, the results of the phase correction method applied for the compensation of the nonlinearity of the swept laser source in our SS-OCT, are described. An example of up-sampled interferogram is shown in Fig. 4. As it can be seen, the signal over the first 2,000 samples is not regular and equidistant (chirped). We use interpolation for up-sampling and averaging for down sampling.

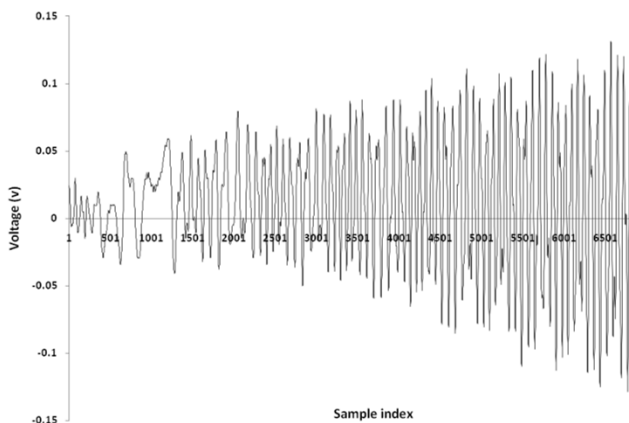


Fig. 4. Interferogram signal obtained when a triangular signal (slope of each sample is one) was sent to the filter. The number of samples in this

signal has been increased by a factor of 10 using the spline interpolation technique.

The zero crossing profile obtained from the interferogram signal is presented in Fig. 5. The height and width of each sample in this graph, demonstrates the distance between two consecutive zeros.

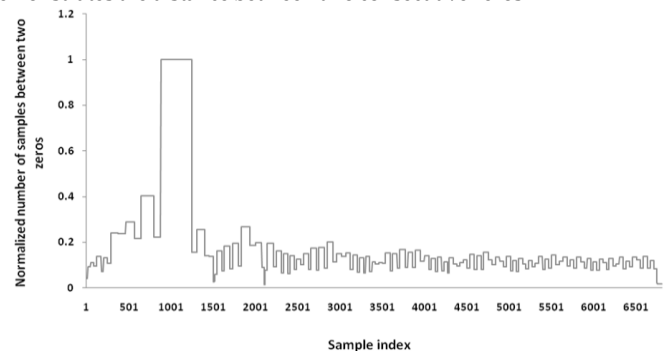


Fig. 5. Zero crossing profile of the interferogram given in Fig. 4.

The ramp signals after the modification using methods #1 and #2 described in section 2, are presented in Fig. 6. The ramp signals were down-sampled from 7000 samples to 100 samples.

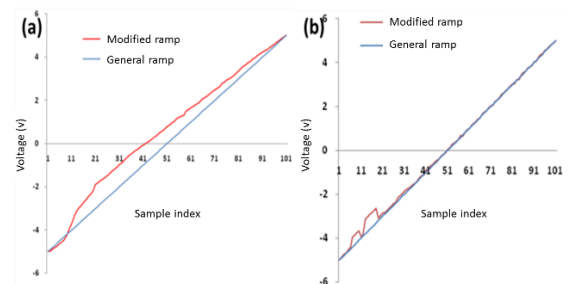


Fig. 6. Constructed ramp signal using the zero crossing profile shown in Fig. 5, after down-sampling: (a) using the method, $sample(i) = sample(i-1) + i * slope_add$, (b) using the method, $sample(i) = i * (1 + slope_add)$. $slope_add$, is the slope obtained from the zero crossing profile.

The modified ramp signal is applied to the filter. The ramp signal that was constructed using the second approach, generates a better equidistant interferogram signal. This is due to the fact that in the first approach adding values to the slope of each sample, increases the height of the signal. Thus, normalizing the resultant signal changes the already determined slopes of the short lines. The interferogram signal obtained from the ramp shown in Fig. 6 (b), is illustrated in Fig. 7. The equally spaced peaks in this interferogram are better than those obtained with the triangular signal. This is shown in the zero crossing profile in Fig. 8. The zero crossing profile in this figure shows a more regular pattern. As shown in Fig. 7, the samples at the beginning of the signal are not as strong as the other samples. This can be the consequence of using too large slopes in the modified ramp signal for this part of the interferogram.

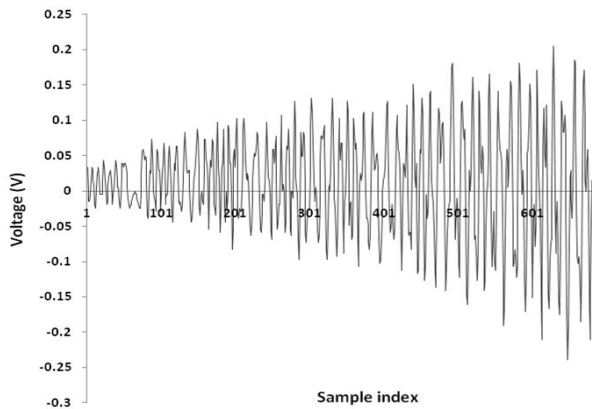


Fig. 7. The interferogram signal after phase correction and after downsampling.

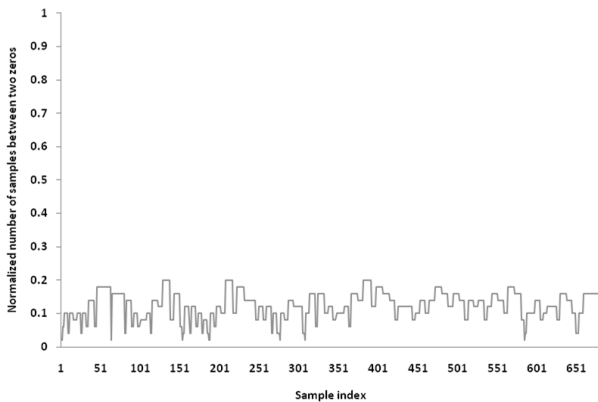


Fig. 8. Zero crossing profile of the interferogram given in Fig. 7 after phase correction.

The FFT of the interferogram of the original signal and the phase corrected signal at two OPD values: 66 μm , and 500 μm , are given in Fig. 9 (a), and (b). There is improvement in the FFT profiles of the interferogram signals. According to the results obtained, the phase correction approach does not improve the nonlinearity of the FP-TF as well as the iterative optimization technique [23]. This may be due to the simplification in the zero crossing algorithm.

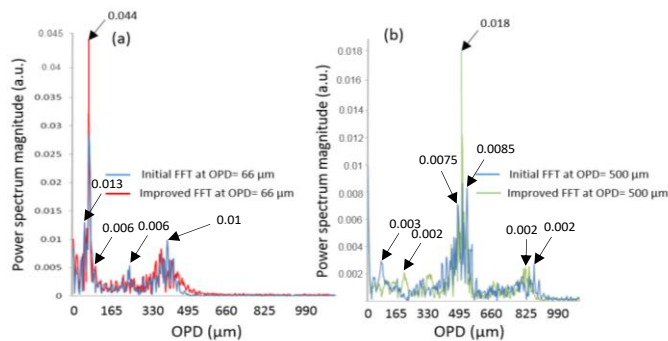


Fig. 9. FFT magnitude before and after correction at a frequency rate of $f=7.2$ kHz applied to the FP filter for two different OPD values: (a) OPD=66 μm , and (b) OPD=500 μm .

The phase correction algorithm performs better for the middle range OPDs, e.g., around 500 μm . The number of slopes is an important factor in the phase correction method. We found that a number of 50 slopes to be optimum for constructing a ramp signal. The optimum number of slopes was obtained using simulated annealing optimization algorithm.

We comprehensively explained the use of this algorithm in [23]. A comparison between our proposed method and the standard phase correction method showed 3 fold speed improvement.

4. CONCLUSION

In this paper, we studied a phase correction method for compensation of the nonlinearity of swept laser sources based on fibre Fabry-Perot tunable filter. We tested the algorithm for the frequency rate of 7.2 kHz at OPD values of 66 μm , and 500 μm . We observed that the algorithm performs better in the middle range OPDs. The number of slopes is an important factor in this method. It was found out that 50 to be an optimum number of slopes in the construction of a ramp signal using simulated annealing optimization algorithm. However, there is a significant improvement in the FFT profiles of the interferogram signals after compensation using this method, the iterative optimization technique still outperformed. As a future work, a more sophisticated algorithm to find the zero crossings more accurately and hence to improve the results of the phase correction method will be designed.

Acknowledgment. We thank Dr Irina Trifanov from Coherent and Antonio Lobo from the Health Sciences, University Fernando Pessoa, Porto, Portugal, for their insightful comments. A. Podoleanu is supported by the NIHR Biomedical Research Centre at Moorfields Eye Hospital NHS Foundation Trust, UCL Institute of Ophthalmology, the European Industrial Doctorate UBAPHODESA 607627 and the Royal Society Wolfson Research Merit Award.

References

1. S. Vergnole, D. Levesque, and G. Lamouche, "Experimental validation of an optimized signal processing method to handle non-linearity in swept-source optical coherence tomography," *Opt Express* **18**, 10446-10461 (2010).
2. M. R. Avnaki, A. Hojjatoleslami, M. Sira, J. B. Schofield, C. Jones, and A. G. Podoleanu, "Investigation of basal cell carcinoma using dynamic focus optical coherence tomography," *Applied optics* **52**, 2116-2124 (2013).
3. Grulkowski, I., Liu, J.J., Potsaid, B., Jayaraman, V., Lu, C.D., Jiang, J., Cable, A.E., Duker, J.S. and Fujimoto, J.G., 2012. Retinal, anterior segment and full eye imaging using ultrahigh speed swept source OCT with vertical-cavity surface emitting lasers. *Biomedical optics express*, 3(11), pp.2733-2751.
4. M. A. Choma, K. Hsu, and J. A. Izatt, "Swept source optical coherence tomography using an all-fiber 1300-nm ring laser source," *Journal of biomedical optics* **10**, 44009 (2005).
5. M. Choma, M. Sarunic, C. Yang, and J. Izatt, "Sensitivity advantage of swept source and Fourier domain optical coherence tomography," *Opt Express* **11**, 2183-2189 (2003).
6. V. V. Tuchin, *Coherent-Domain Optical Methods: Biomedical Diagnostics, Environment and Material Science* (Springer Science & Business Media, 2004).
7. A. Hojjatoleslami and M. R. Avnaki, "OCT skin image enhancement through attenuation compensation," *Applied optics* **51**, 4927-4935 (2012).
8. M. R. Avnaki, A. G. Podoleanu, J. B. Schofield, C. Jones, M. Sira, Y. Liu, and A. Hojjat, "Quantitative evaluation of scattering in optical coherence tomography skin images using the extended Huygens-Fresnel theorem," *Applied optics* **52**, 1574-1580 (2013).
9. S. Hojjatoleslami, M. Avnaki, and A. G. Podoleanu, "Image quality improvement in optical coherence tomography using Lucy-Richardson deconvolution algorithm," *Applied optics* **52**, 5663-5670 (2013).
10. Nakazaki, Y. and Yamashita, S., 2009. Fast and wide tuning range wavelength-swept fiber laser based on dispersion tuning and its application to dynamic FBG sensing. *Optics express*, 17(10), pp.8310-8318.

11. I. Trifanov, A. Bradu, L. Neagu, P. Guerreiro, A. L. Ribeiro, and A. G. Podoleanu, "Experimental method to find the optimum excitation waveform to quench mechanical resonances of Fabry–Pérot tunable filters used in swept sources," *IEEE Photonics Technology Letters* **23**, 825-827 (2011).
12. T.-J. Ahn, J. Y. Lee, and D. Y. Kim, "Suppression of nonlinear frequency sweep in an optical frequency-domain reflectometer by use of Hilbert transformation," *Applied optics* **44**, 7630-7634 (2005).
13. S. S. Sherif, C. Fluoraru, Y. Mao, and S. Change, "Swept source optical coherence tomography with nonuniform frequency domain sampling," in *Biomedical Optics*, (Optical Society of America, 2008), BMD86.
14. J. Xi, L. Huo, J. Li, and X. Li, "Generic real-time uniform K-space sampling method for high-speed swept-Source optical coherence tomography," *Optics express* **18**, 9511-9517 (2010).
15. M. Y. Jeon, J. Zhang, and Z. Chen, "Characterization of Fourier domain modelocked wavelength swept laser for optical coherence tomography imaging," *Optics express* **16**, 3727-3737 (2008).
16. C. M. Eigenwillig, B. R. Biedermann, G. Palte, and R. Huber, "K-space linear Fourier domain mode locked laser and applications for optical coherence tomography," *Optics express* **16**, 8916-8937 (2008).
17. Huang, S.W., Aguirre, A.D., Huber, R.A., Adler, D.C. and Fujimoto, J.G., 2007. Swept source optical coherence microscopy using a Fourier domain mode-locked laser. *Optics express*, 15(10), pp.6210-6217.
18. M. R. Avanaki, A. G. Podoleanu, M. C. Price, S. A. Corr, and S. A. Hojjatoleslami, "Two applications of solid phantoms in performance assessment of optical coherence tomography systems," *Applied optics* **52**, 7054-7061 (2013).
19. M. Nasirivanaki, J. Xia, H. Wan, A. Q. Bauer, J. P. Culver, and L. V. Wang, "High-resolution photoacoustic tomography of resting-state functional connectivity in the mouse brain," *Proceedings of the National Academy of Sciences* **111**, 21-26 (2014).
20. R. Huber, M. Wojtkowski, K. Taira, J. Fujimoto, and K. Hsu, "Amplified, frequency swept lasers for frequency domain reflectometry and OCT imaging: design and scaling principles," *Optics Express* **13**, 3513-3528 (2005).
21. M. R. Avanaki, A. Bradu, I. Trifanov, A. B. L. Ribeiro, A. Hojjatoleslami, and A. G. Podoleanu, "Algorithm for excitation optimization of Fabry–Pérot filters used in swept sources," *IEEE Photonics Technology Letters* **25**, 472-475 (2013).
22. Trifanov, I., Neagu, L., Bradu, A., Ribeiro, A.L. and Podoleanu, A.G., 2011, February. Characterization of a fibre optic swept laser source at 1 μm for optical coherence tomography imaging systems. In *SPIE BiOS* (pp. 78892T-78892T). International Society for Optics and Photonics.
23. Nasiri-Avanaki, M.R., Hojjatoleslami, S., Paun, H., Tuohy, S., Meadway, A., Dobre, G. and Podoleanu, A., 2009, September. Optical coherence tomography system optimization using simulated annealing algorithm. In *Proceedings of Mathematical Methods and Applied Computing* (pp. 669-674).